Title: Electrical synapse formation is differentially regulated by distinct isoforms of a postsynaptic scaffold

Authors: Jennifer Carlisle Michel, Margaret M. B. Grivette, Amber T. Harshfield, Lisa Huynh, Ava P. Komons, Bradley Loomis, Kaitlan McKinnis, Brennen T. Miller, Ethan Q. Nguyen, Tiffany W. Huang, Sophia Lauf, Elias S. Michel, Mia E. Michel, Audrey J. Marsh, Lila E. Kaye, Abagael M. Lasseigne, Rachel M. Lukowicz-Bedford, Dylan R. Farnsworth, E. Anne Martin, Adam C. Miller*

* = corresponding author
Institute of Neuroscience, University of Oregon, United States

Abstract
Electrical synapses are neuronal gap junction (GJ) channels associated with a macromolecular complex called the electrical synapse density (ESD), which regulates development and dynamically modifies electrical transmission. However, the proteomic makeup and molecular mechanisms utilized by the ESD that direct electrical synapse formation are not well understood. Using the Mauthner cell of zebrafish as a model, we previously found that the intracellular scaffolding protein ZO1b is a member of the ESD, localizing postsynaptically, where it is required for GJ channel localization, electrical communication, neural network function, and behavior. Here, we show that the complexity of the ESD is further diversified by the genomic structure of the ZO1b gene locus. The ZO1b gene is alternatively initiated at three transcriptional start sites resulting in isoforms with unique N-termini that we call ZO1b-Alpha, -Beta, and -Gamma. We demonstrate that ZO1b-Beta and ZO1b-Gamma are broadly expressed throughout the nervous system and localize to electrical synapses. By contrast, ZO1b-Alpha is expressed mainly non-neuronally and is not found at synapses. We generate mutants in all individual isoforms, as well as double mutant combinations *in cis* on individual chromosomes, and find that ZO1b-Beta is necessary and sufficient for robust GJ channel localization. ZO1b-Gamma, despite its localization to the synapse, plays an auxiliary role in channel localization. This study expands the notion of molecular complexity at the ESD, revealing that an individual genomic locus can contribute distinct isoforms to the macromolecular complex at electrical synapses. Further, independent scaffold isoforms have differential contributions to developmental assembly of the interneuronal GJ channels. We propose that ESD molecular complexity arises both from the diversity of unique genes and from distinct isoforms encoded by single genes. Overall, ESD proteomic diversity is expected to have critical impacts on the development, structure, function, and plasticity of electrical transmission.

Introduction

Fast synaptic transmission in the nervous system is mediated by electrical and chemical synapses, with each type imparting distinct modes of communication (Moroz and Kohn, 2016; Pereda, 2014; Ryan and Grant, 2009). Electrical synapses directly couple neurons via interneuronal gap junction (GJ) channels, whereas chemical synapses utilize neurotransmitter release/reception for signaling. Despite unique structures and functions, both synaptic types are supported by locally-assembled, cytoplasmic, associated proteins that regulate the development and function of transmission. At chemical synapses, hundreds of proteins are associated with the presynaptic active zone (AZ) and postsynaptic density (PSD) and regulate synaptic vesicle release and neurotransmitter localization, respectively (Ackermann et al., 2015; Grant, 2019; Patel et al., 2006; Siddiqui and Craig, 2011). Critical to the structure and function of glutamatergic chemical synapses is a family of postsynaptic membrane-associated guanylate kinases (MAGUKs) that coordinate and link the macromolecular construction of the cytoplasmic PSD structure to the membrane localization and function of NMDA and AMPA receptors (Zheng et al., 2011; Zhu et al., 2016). By contrast, few electrical synapse-associated proteins have been identified to date, yet electron micrographs of neuronal tissue suggest a cytoplasmic, GJ-associated regulatory network complementing each side of electrical synapses (Brightman and Reese, 1969; Kimmel et al., 1981), and we have termed these structures the electrical synapse density (ESD). Our recent work revealed that the ESD component ZO1b, a MAGUK intracellular scaffolding protein, localizes postsynaptically at zebrafish electrical synapses where it directly interacts with neuronal GJ-channel forming Connexins, and is required for GJ-channel localization, electrical communication, neural network function, and behavior (Lasseigne et al., 2021). Yet the proteomic diversity found at the ESD and how it controls electrical synapse formation remains poorly understood.

Synaptic proteomic diversity can arise from both unique gene products as well as distinct isoforms of individual genes. At glutamatergic chemical synapses, the alternative transcriptional initiation of postsynaptic MAGUKs creates distinct protein isoforms with unique N-terminal domains that result in differential regulation and activity. For example, the MAGUK protein SAP97 exists as two alternatively-initiated isoforms, α and β. The SAP97α-isoform is palmitoylated on its unique N-terminal domain, targeting the isoform to the PSD. The SAP97β-isoform encodes an L27 interaction domain that targets this isoform to the non-PSD, perisynaptic region. Expression of these different SAP97 isoforms allows distinct classes of associated complexes to control the subsynaptic distribution of AMPA receptors, consequently affecting synaptic strength (Goodman et al., 2017; Waites et al., 2009). By contrast, there are no reports revealing similar isoform-specific contributions to ESD proteomic diversity, yet the ESD-associated ZO1 is better known for its role in regulating epithelial tight junction (TJ) structure and function (González-Mariscal et al., 2000). In epithelia, two isoforms of ZO1 arise from alternative splicing, are associated with antomically-distinct TJs, and cause isoform-dependent effects on junctional plasticity that alter epithelial barrier function (Balda and Anderson, 1993; Willot et al., 1992). These observations suggest that unique isoforms of ESD proteins may have distinct spatiotemporal and functional motifs that control the structure and function of electrical synapses.

Here we identify an alternative initiation mechanism of ZO1b that regulates electrical synapse diversity and development. We investigate three independent transcriptional start sites of the ZO1b-encoding gene, hereafter called ZO1b-Alpha, -Beta, and-Gamma, and use genetics, transgenics, and imaging to elucidate their contributions and functions in the Mauthner cell neural circuit of zebrafish. The results expand the proteomic complexity of the ESD and reveal that unique isoforms encoded from a single gene can have differential effects on the structure and function of electrical synapse formation. This emerging complexity of ESD proteins and functions at the electrical synapse parallels findings at chemical synapses where unique scaffold isoforms play distinct functions in the structure, function, and plasticity of synaptic transmission.

Results

Alternatively initiated isoforms of the *tjp1b/ZO1b gene* are expressed in the Mauthner cell circuit

At electrical synapses, interneuronal gap junction (GJ) channels are formed by the docking of two hemichannels, composed of Connexin proteins in vertebrates (Söhl et al., 2005). Hemichannels are contributed by each of the coupled neurons to create the interconnecting channel, forming a direct path of communication that allows the spread of electrical currents and small metabolites between neurons. Our recent work demonstrated that the ZO1b intracellular scaffold is required postsynaptically for Connexin localization at zebrafish Mauthner cell electrical synapses (Fig.1A)(Lasseigne et al., 2021; Marsh et al., 2017). Located on chromosome 25, the *tjp1b* gene encodes the ZO1b protein (*tjp1b/ZO1b)*, and the locus is complex with three distinct initiation sites annotated on public databases (Ensembl, ENSDARG00000079374) that predict three transcripts of varying lengths (Fig. 1B). Each transcript contains a unique first exon, including distinct 5' untranslated regions (UTRs) and translational start codons, and each has a varying number of additional exons incorporated before splicing into a common exon and the subsequent remaining transcript and 3' UTR (Fig. 1C). While each transcript predicts a unique N-terminal peptide sequence, all three retain the assortment of common MAGUK protein-protein interaction modules including PDZs, SH3, GUK, and ZU5 domains (Fig. 1C). This genomic structure spurred us to examine if *tjp1b/ZO1b* transcriptional initiation complexity contributes to electrical synapse proteomic diversity.

To examine how alternatively initiated transcripts might contribute to Mauthner electrical synapses, we first inspected the spatiotemporal expression pattern of *tjp1b/ZO1b* through early development using our single cell RNA-seq (scRNA-seq) atlas (Farnsworth et al., 2020; Lukowicz-Bedford et al., 2022). The atlas revealed broad expression of the *tjp1b/ZO1b* transcript in neural and non-neural cells from 1 to 5 days post fertilization (dpf), suggesting broad usage of the gene in different tissues over time (Fig. S1A). This broad expression was expected given ZO1's known roles in tight junction formation in epithelial tissues (Balda and Anderson, 1993; González-Mariscal et al., 2000; Stevenson et al., 1986). While the atlas data suggests expression in developing neurons (Fig. S1A), the chemistry used for the scRNA-seq (10X Genomics) is biased toward the 3' end of genes preventing analysis of the alternatively initiated

transcripts. Therefore, we designed probes to detect the unique first exons of each isoform and used fluorescent RNA *in situ* on wildtype 5 dpf whole zebrafish. We observed robust expression of *tjp1b/ZO1b-Beta* and *tjp1b/ZO1b-Gamma* transcripts in the brain and spinal cord, yet little evidence for neuronal *tjp1b/ZO1b-Alpha* expression (Fig. S1B). We also observed overlapping expression for the isoforms in other areas, such as skin, otolith, and jaw (Fig. S1B). From these data we conclude that *tjp1b/ZO1b-Beta* and *tjp1b/ZO1b-Gamma* transcripts are the main isoforms expressed in neuronal tissue.

We next addressed which *tjp1b/ZO1b* isoforms are expressed in neurons of the Mauthner circuit, as the Mauthner neuron and its synapses are an ideal model to understand electrical synapse formation (Fig.1A). This circuit drives a fast escape response to threatening stimuli and is composed of two Mauthner cells in each animal that receive multimodal sensory input that is then relayed to spinal cord circuitry (Eaton et al., 1977; Jacoby and Kimmel, 1982; Liu and Fetcho, 1999). Mauthner makes prominent, stereotyped, electrical synapses with auditory afferents on its lateral dendrite (Club endings, CEs) (Bartelmez and Hoerr, 1933; Pereda et al., 2004; Yao et al., 2014). Additionally, the Mauthner axons make electrical synapses with Commissural Local (CoLo) interneurons of the spinal cord (M/CoLo) (Satou et al., 2009). We looked for *tjp1b/ZO1b* isoform expression in 5 dpf fish harboring the enhancer trap transgene *zf206Et* that expresses GFP in both Mauthner and CoLo cells (Fig. 1D-K). Signals for *tjp1b/ZO1b-Beta* and *tjp1b/ZO1b-Gamma* transcripts were readily observed in both Mauthner and CoLo cell bodies (Fig. 1H-K). We note that much of the fluorescent signal appeared as two distinct puncta within the nuclei of the neurons, similar to other reported RNAs that accumulate into discrete nuclear granules in neuronal cell bodies (Casafont et al., 2010; Narcís et al., 2018). Signal for *tjp1b/ZO1b-Alpha* transcript was not detected in Mauthner or CoLo but was expressed at low levels in unidentified nearby cells in the neural tube (white arrow, Fig. 1F,G), suggesting it may play a role in cells outside of the Mauthner circuit. We conclude that *tjp1b/ZO1b-Beta* and *tjp1b/ZO1b-Gamma* are expressed in Mauthner and CoLo, making them electrical synapse candidates.

ZO1b-Beta and ZO1b-Gamma localize to electrical synapses

We next determined if distinct transcripts lead to unique protein expression in the Mauthner cell circuit. To achieve this we used CRISPR to insert a V5 epitope tag at the N-terminus of each *tjp1b/ZO1b* isoform and looked for V5 immunostaining in the Mauthner cell circuit of 5 dpf larvae (V5 insertion locations shown in Fig. 1B). First, we found that using CRISPR/Cas9-induced homology directed repair with a short, single-stranded nucleotide repair oligo resulted in animals with frequent insertion of the V5 epitope tag into the locus of interest (Fig. S1C-E). Examining injected animals with mosaically labeled ZO1b isoforms, we found that both V5-ZO1b-Beta and V5-ZO1b-Gamma were localized to Mauthner electrical synapses (Fig. S1D,E). Within the Mauthner circuit, neuronal GJs at both CEs and M/CoLo synapses are made of heterotypic channels formed by Cx35.5, encoded by the gene *gap junction delta 2a* (*gjd2a*), and Cx34.1, encoded by *gjd1a* – both homologous to mammalian Cx36 (*gjd2*) and both recognized by the antibody against human Cx36 (Miller et al., 2017). In V5-

ZO1b-Beta and V5-ZO1b-Gamma injections, anti-V5 staining was found to colocalize with anti-Cx36 staining at M/CoLo synapses. By contrast, for V5-ZO1b-Alpha, none of the injected embryos mosaically expressed V5-ZO1b-Alpha in any tissue examined including the nervous system, despite 100% of sibling fish being successfully targeted as determined by PCR analysis (Fig. S1C). While this suggests that ZO1b Alpha plays no role at Mauthner electrical synapses, it is possible that either no in-frame repairs were made or that V5-ZO1b-Alpha is not expressed at the developmental stage examined. Given the mosaic results, we generated transgenic lines (*V5-tjp1b-Beta*^{b1406} and *V5-tjp1b-Gamma*^{b1449}) and observed localization of V5-ZO1b-Beta and V5-ZO1b-Gamma proteins at the stereotyped locations of CE and M/CoLo electrical synapses (Fig. 1L-O). V5-ZO1b-Beta and V5-ZO1b-Gamma colocalized with neuronal Cx34.1 and Cx35.5 staining at the synaptic contacts and both Beta and Gamma isoforms were distributed with the unique morphological shape of the Mauthner electrical synapses (Fig. 1L-O). The localization of both Beta and Gamma isoforms is reminiscent of electrical synaptic ZO1 staining observed using anti-ZO1 antibody (Lasseigne et al., 2021; Marsh et al., 2017). Finally, we also observed V5-ZO1b-Beta and V5-ZO1b-Gamma at non-neuronal epithelial cell junctions (Fig. S1F,G) and V5-ZO1b-Beta was observed throughout the nervous system colocalized with Connexin staining (Fig. S1H). We conclude that both V5-ZO1b-Beta and V5-ZO1b-Gamma are localized to Mauthner electrical synapses.

ZO1b-Beta is required for robust synaptic Connexin localization

The protein sequences from the three *tjp1b/ZO1b* transcripts predict unique N-terminal peptide sequences for each, though only ZO1b-Alpha has an identifiable domain, a caspase activation and recruitment domain (CARD), while ZO1b-Beta and ZO1b-Gamma have sequences that fail to predict function (Fig. 1C, Fig. S2A). The common portion of all isoforms retain the PDZ1 binding domain (Fig. 1C), which we previously demonstrated mediates direct biochemical interaction with Cx34.1 (Lasseigne et al., 2021). We first asked whether differential N-terminal sequences would affect Cx34.1 binding by cloning full-length sequences of *tjp1b/ZO1b-Alpha, tjp1b/ZO1b-Beta,* and *tjp1b/ZO1b-Gamma* and using heterologous expression to test for interactions. HEK293T cells were co-transfected with individual ZO1b isoforms and full-length Cx34.1. Using Western blot analysis with antibodies specific to ZO1 and Cx34.1, we found that Cx34.1 was detected in all ZO1b isoform immune complexes compared to control immunoprecipitate (Fig. S2B). We conclude that each unique ZO1b isoform can interact with zebrafish Cx34.1.

Next, we examined the role of each ZO1b isoform at electrical synapses *in vivo* using CRISPR/Cas9-induced mutations to knock out individual isoforms. We generated mutant lines that introduced frame-shifts and early stop codons in each of the first coding exons of the isoforms and analyzed antibody staining for Cx35.5, Cx34.1, and ZO1 at Mauthner circuit electrical synapses using immunohistochemistry at 5 dpf (Fig. 2A-J). We compared these individual-isoform mutants to a “pan” mutation in the first common exon shared by the *alpha, beta, and gamma* transcripts (CRISPR mutations associated with particular alleles are identified in Fig. 1B). In *tjp1b/ZO1b-pan*$^{-/-}$ mutants we observed nearly undetectable Cx35.5, Cx34.1, and ZO1 antibody staining at the CE

and M/CoLo electrical synapses (Fig. 2C,D). As expected from the expression analysis (Fig. 1,S1), *tjp1b/ZO1b-alpha*$^{-/-}$ mutants had no effect on Connexin or ZO1 staining (Fig. 2E,F). By contrast, in the *tjp1b/ZO1b-beta*$^{-/-}$ mutants there was a dramatic reduction of both Connexins and ZO1 staining at Mauthner electrical synapses (Fig. 2G,H). And despite V5-ZO1b-Gamma protein localizing to electrical synapses (Fig.1N,O), the *tjp1b/ZO1b-gamma*$^{-/-}$ mutants had no apparent effect on Connexin or ZO1 staining at Mauthner circuit synapses (Fig. 2I,J). Quantitation of Cx34.1 at M/CoLo contacts confirmed that staining was greatly diminished in *tjp1b/ZO1b-beta*$^{-/-}$ mutants compared to wildtype and *tjp1b/ZO1b-alpha*$^{-/-}$ and *tjp1b/ZO1b-gamma*$^{-/-}$ isoform mutants (Fig. 2K). Using qPCR we found that both the Alpha and Gamma isoforms were upregulated in the *tjp1b/ZO1b-beta*$^{-/-}$ mutants (Fig. S2C), suggesting that these isoforms might be undergoing transcriptional adaptation (El-Brolosy et al., 2019). Noteably, this shows that the *alpha* and *gamma* isoforms were expressed in the *tjp1b/ZO1b-beta*$^{-/-}$ mutants but were unable to rescue normal synaptic Connexin localization (Fig. 2G,H,K). We conclude that ZO1b-Beta is required for robust Connexin localization at Mauthner electrical synapses.

While greatly diminished, *tjp1b/ZO1b-beta*$^{-/-}$ mutants retained elevated Connexin localization at Mauthner electrical synapses as compared with the *tjp1b/ZO1b-pan*$^{-/-}$ mutants (Fig. 2K, *tjp1b/ZO1b-pan*$^{-/-}$, 3% synaptic Cx34.1, n=3; *tjp1b/ZO1b-beta*$^{-/-}$, 16% synaptic Cx34.1, n=5, p=0.0052, unpaired t-test with Welch's correction). To determine if ZO1b-Gamma plays a role alongside ZO1b-Beta at electrical synapses, we generated *tjp1b/ZO1b-beta-gamma*$^{-/-}$ double mutants and examined Connexin localization at electrical synapses. Note that we generated the Gamma-disrupting mutation on the *tjp1b/ZO1b-beta* mutant chromosome, grew lines of animals carrying both mutations, then analyzed double homozygous mutants that disrupted both Beta and Gamma isoforms (disruptions are induced in exon 1 of both *beta* and *gamma* isoforms, in cis, of the same *tjp1b* gene). In *tjp1b/ZO1b-beta-gamma*$^{-/-}$ double mutants, there was a further loss of synaptic Cx34.1 staining as compared to *tjp1b/ZO1b-beta*$^{-/-}$ mutants alone (Fig. 2K inset box, ~44% decrease, *tjp1b/ZO1b-beta*$^{-/-}$ n=6, *tjp1b/ZO1b-beta-gamma*$^{-/-}$, n=6, p=0.0023, unpaired t-test with Welch's correction), indicating that ZO1b Gamma may play a minor role in scaffolding Connexins at Mauthner electrical synapses. Taken together, we conclude that ZO1b-Beta and ZO1b-Gamma are localized to electrical synapses, yet the Beta isoform is differentially required for the robust localization of Connexins at synaptic contacts during development.

ZO1b-Beta is sufficient for robust Connexin localization to electrical synapses
Next, we examined whether the presence of ZO1b-Beta was sufficient for robust electrical synapse formation. To achieve this we generated double mutants, in cis, amongst each combination of the *tjp1b/ZO1b-alpha*, *-beta*, and *-gamma* isoforms. For double mutants that retained the *tjp1b/ZO1b-beta* isoform we expected to see synaptic Connexin localization, while those lacking the *beta* isoform were expected to show a loss of synaptic Connexin. Indeed, in *tjp1b/ZO1b-alpha-gamma*$^{-/-}$ double mutants, in which the Beta isoform remains intact, Cx35.5, Cx34.1 and ZO1 were robustly localized to CE and M/CoLo synapses as compared with wildtype fish (Fig. 3A-D). By contrast, in *tjp1b/ZO1b-alpha-beta*$^{-/-}$ and *tjp1b/ZO1b-beta-gamma*$^{-/-}$ double mutants, there was

decreased signal for Cx35.5, Cx34.1 and ZO1 antibody staining at Mauthner circuit electrical synapses (Fig. 3E-H). Quantitation of Cx34.1 at M/CoLo contacts revealed that *tjp1b/ZO1b-alpha-gamma*$^{-/-}$ double mutants had an increase in Connexin localization as compared to wildtype (Fig. 3I, ~37% increase, wildtype n=15, *tjp1b/ZO1b-alpha-gamma*$^{-/-}$ n=5, p=0.0186, unpaired t-test with Welch's correction), while *tjp1b/ZO1b-alpha-beta*$^{-/-}$ and *beta-gamma*$^{-/-}$ double mutants had significant loss of synaptic Connexin compared to wildtype (Fig. 3I, ~19%, wildtype n=15, *tjp1b/ZO1b-alpha-beta*$^{-/-}$ n=5, p<0.0001, unpaired t-test with Welch's correction; and ~23% , wildtype n=15, *tjp1b/ZO1b-beta-gamma*$^{-/-}$ n=5, p<0.0001, unpaired t-test with Welch's correction, respectively). Given that we found this locus upregulates related isoforms in mutants (Fig. S2C), the observed relative increase of synaptic Connexin localization in the *tjp1b/ZO1b-alpha-gamma*$^{-/-}$ double mutants may be accounted for by transcript upregulation of the *tjp1b/ZO1b-beta* isoform in the double mutants. From these observations we conclude that the presence of ZO1b-Beta is sufficient for robust Connexin localization at electrical synapses. Taken together, these results provide evidence that both ZO1b-Beta and ZO1b-Gamma are localized to electrical synapses, yet the Beta isoform appears to distinctly license Connexin localization to the synapse during development.

Discussion

The results presented here reveal that a single genomic locus can encode unique ESD scaffold isoforms with differential effects at the electrical synapse. Our findings show that ZO1b-Beta is the dominant isoform functioning to localize Connexins to Mauthner electrical synapses during development, while ZO1b-Gamma is present but has only a minor accessory role. These findings reveal that protein diversity at the electrical synapse can be encoded by unique isoforms of individual gene loci. We note that both the Beta and Gamma isoforms were also observed to be colocalized with neural Connexins throughout the nervous system, yet disruption of the Beta-isoform, but not the Gamma, resulted in a loss of gross synaptic Connexin localization across the brain (data not shown). How this differential effect occurs, with Beta being the dominant scaffold required for developmental Connexin localization, is not currently clear. One possibility is that ZO1b-Beta is present at a much higher concentration at the electrical synapse as compared to Gamma. While we detected each ZO1b isoform at electrical synapses using the V5 tag, comparing their relative levels would require unique detection reagents such as alternative epitope tags (e.g., FLAG, HA, etc), which have not been successful in our experiments to date. If differential expression levels explain the distinct effects on Connexin localization, then expression must be controlled by unique genomic elements upstream of each transcriptional start site (TSS). Currently, there is little known about the transcriptional control of vertebrate electrical synapse formation (Martin et al., 2003). Alternatively, the unique amino acids of each isoform may impart distinct functions, perhaps by affecting the functional interactions of ZO1 with Connexins or other ESD proteins at the synapse, or by affecting the sub-synaptic targeting of ZO1. This would be analogous to the effects seen for SAP97 and PSD95 at glutamatergic chemical synapses, where unique scaffold isoforms play distinct functions in synapse development, neurotransmitter receptor localization, and plasticity (Araki et al., 2020; Goodman et al., 2017; Hirao et al., 2000; Waites et al., 2009). By analogy, it is

intriguing to speculate that the Beta and Gamma isoforms could play unique roles at the electrical synapse. We have demonstrated that ZO1b-Beta is necessary and sufficient for robust Connexin localization during development, and perhaps ZO1b-Gamma could be used to modulate an alternative function, such as electrical synapse plasticity (Alcamí and Pereda, 2019; Arroyo et al., 2016; Bhattacharya et al., 2019; Bloomfield and Völgyi, 2009; Marder, 1998; O'Brien, 2019). Finally, we note that our experiments cannot exclude the possibility that other unique TSS isoforms may play a role, perhaps explaining the residual Connexin localization in the *tjp1b/ZO1b-alpha-beta*$^{-/-}$ and *tjp1b/ZO1b-beta-gamma*$^{-/-}$ double mutants. Future experiments that reveal the relative contributions of each isoform, and that probe electrical synapse homeostasis, transmission, and plasticity, will reveal how the isoform-complexity of ZO1b at the electrical synapse regulates structure and function.

An ongoing barrier in the field of electrical synapses is the lack of knowledge surrounding the proteomic makeup of the ESD and how these proteins regulate synapse assembly. Our working model is that ESD complexity comprises multiple unique classes of proteins, including cell adhesion, scaffolds, and regulatory molecules (Martin et al., 2020; Miller and Pereda, 2017). Our previous work revealed that ZO1b is an exclusively postsynaptic member of the ESD, where it binds Connexins, and is necessary and sufficient for channel localization and function (Lasseigne et al., 2021). Our findings here reveal that we must further consider unique isoforms of each of the ESD proteins. Though we focused on ZO1b isoforms resulting from alternative transcriptional initiation, there are many predicted alternatively spliced forms of downstream exons (NCBI) that are likely to alter protein-protein interaction domains – these may add further complexity to building functional electrical synapses. Finally, mammalian ZO1 is known to localize to electrical synapses throughout the brain (Li et al., 2004) and the mammalian ZO1 is documented to have multiple isoforms, arising from both unique transcriptional start sites and alternative splicing (Balda and Anderson, 1993; Willot et al., 1992). This supports the notion that unique ESD isoforms could create electrical synapse proteomic and functional diversity and may be a general feature of vertebrate brains. Thus, ESD complexity, even when viewed only at the level of ZO1b scaffold isoforms, is certainly vastly underestimated. Overall, we expect that ESD complexity will be derived from both discrete classes of molecules as well as unique protein isoforms of the same gene, each with distinct impacts on electrical synapse formation, function, and plasticity.

Materials and Methods

Zebrafish

Fish were maintained in the University of Oregon fish facility with approval from the Institutional Animal Care and Use Committee (IACUC AUP 21-42). Zebrafish, *Danio rerio*, were bred and maintained at 28 °C on a 14 hr on and 10 hr off light cycle. Animals were housed in groups, generally of 25 animals per tank. Development time points were assigned via standard developmental staging (Kimmel et al., 1995). All fish used for this project were maintained in the ABC background developed at the University of Oregon. Most fish had the enhancer trap transgene *zf206Et (M/CoLo:GFP)* in the background

(Satou et al., 2009), unless otherwise noted. The *V5-tjp1b-Beta*^{b1406} line contains an in-frame NH_2-V5 affinity tag in the exon encoding the *tjp1b/ZO1b-beta* isoform (Lasseigne et al., 2021). The *V5-tjp1b-Gamma*^{b1449} line contains an in-frame NH_2-V5 affinity tag in the exon encoding *tjp1b/ZO1b-gamma* isoform. The *tjp1b-pan*^{b1370} mutant line contains a 16 bp deletion in the *tjp1b* gene (common Exon 5, affecting all isoforms) (Marsh et al., 2017). The *tjp1b-alpha*^{b1429} mutant line contains an 8 bp deletion in the *tjp1b/ZO1b-alpha* first exon. The *tjp1b-beta*^{b1430} mutant line contains a 16 bp insertion in the *tjp1b/ZO1b-beta* first exon. The *tjp1b-gamma*^{b1431} mutant line contains a 7 bp deletion in the *tjp1b/ZO1b-gamma* first exon. The *tjp1b-alpha-beta*^{b1432} double mutant line was generated using the *tjp1b-beta*^{b1430} line and in addition contains an 8 bp deletion in the *tjp1b-alpha* first exon on the same chromosome. The *tjp1b-beta-gamma*^{b1433} double mutant was generated using the *tjp1b-beta*^{b1430} line and in addition contains an 11 bp deletion in the *tjp1b-gamma* first exon on the same chromosome. The *tjp1b-alpha-gamma*^{b1434} double mutant line was generated using the *tjp1b-alpha*^{b1429} line and in addition contains a 4 bp deletion in the *tjp1b-Gamma* first exon on the same chromosome. Mutant lines were genotyped for all experiments. All immunohistochemistry and RNA *in situ* analyses were performed at 5 dpf. At this stage of development, zebrafish sex is not yet determined (Wilson et al., 2014).

Cas9-mediated genome engineering of *tjp1b/ZO1b* isoform mutants

Single guide RNAs (sgRNAs) targeting isoform specific Exon 1 of *tjp1b/ZO1b-alpha, -beta,* and *-gamma* were designed using the CRISPRscan algorithm (Moreno-Mateos et al., 2015) and synthesized as previously described (Shah et al., 2015) using the T7 megascript kit (ThermoFisher).

The CRISPR target sequences used to create mutants for each isoform (PAM underlined) are as follows: *tjp1b Alpha,* 5'-GAGCGGGAGGAGGAATAAACGGG-3'; *tjp1b Beta,* 5'-GTTTTCTGGGAGGCAGGCTACGG-3'; and *tjp1b Gamma,* 5'-TGCCCGGGCTGCCTCTAATAAGG -3'.

Injection mixes were prepared in a pH 7.5 buffer solution of 300 mM KCl and 4 mM HEPES and contained a final concentration of 1-6 uM sgRNA and 10uM Cas9 protein (IDT). Injection mixes were incubated at 37 °C for 5 min immediately prior to injection to promote formation of the Cas9 and sgRNA complex. Embryos containing the enhancer trap transgene *zf206Et (M/CoLo:GFP)* were injected with 1 nL at the one-cell stage (Burger et al., 2016). Injected embryos were raised to adulthood and outcrossed to wild-type animals. Animals carrying gene-disrupting mutations were identified and verified using PCR and Sanger sequencing. Generating double mutant lines required disrupting each gene on the same chromosome. To generate the isoform double mutant lines, we injected animals carrying known/sequenced mutations in individual isoforms with sgRNAs targeting other isoforms to generate mutations in cis on the same chromosome. For details on lines/lineages, see Zebrafish section above. Confirmation of double mutants in cis were verified by sequencing.

Cas9-mediated genome engineering of *V5-tjp1b/ZO1b* isoform mosaics and lines

The *V5-tjp1b/ZO1b* isoform-specific single-stranded donor oligos (ssODN) were designed to repair into the respective endogenous *tjp1b/ZO1b* loci. The ssODN contained ~40 bp homology arms which flanked an XbaI restriction site, V5 sequence, and a 5x glycine linker. If the inserted sequence did not disrupt the endogenous sgRNA recognition site, mutations were designed in the CRISPR/PAM sites of the ssODN to prevent further double stranded breaks after repair.

The CRISPR target sequences used to insert N-terminal V5 coding sequence for each isoform (PAM underlined) are as follows:
tjp1b Alpha: 5'-ATGCTCTTGTCTGTCTTTGGCGG-3';
tjp1b Beta: 5'-GTATTTCTGGTAATTCACCATGG-3';
tjp1b Gamma: 5'-TGCCCGGGCTGCCTCTAATAAGG-3'.

The sequences for the ssODN used to repair each *tjp1b* isoform are as follows:
tjp1b Alpha: Alt-HDR-Modified-5'-
CAAAAATTGCACAGAAATGACCACAAGTCTCTTCTAAAACATGTCTAGAGGCAAAC
CGATTCCGAACCCGCTGCTGGGCCTGGATAGCACCGGAGGTGGAGGCGGACTGC
TGTCAGTGTTCGGGGGACCTGTTGAAGAAGTGTTAGCAGGACTCCTCAAGCTGAA
G-3';
tjp1b Beta: 5-
TGCGGATTTTTGTGTTTCAAAAAAGCGGTGAACAGTACCATGTCTAGAGGCAAACC
GATTCCGAACCCGCTGCTGGGCCTGGATAGCACCGGAGGTGGAGGCGGAGTGAA
TTACCAGAAATACATTACTGTTATGCAGCTGGCTC-3';
tjp1b Gamma: Alt-HDR-Modified-5'-
CTCAACTTGCCTCGGCGCGAGCAGCTAAAGGAACAAAATGTCTAGAGGCAAACCG
ATTCCGAACCCGCTGCTGGGCCTGGATAGCACCGGAGGTGGAGGCGGATCAGCG
CGCGCAGCGTCTAATAAGGTTTGTGCTCATTTATACACATCTCAGACGCATTGTCT
GCAGTTGTCAG-3'.

Injection mixes were prepared in a pH 7.5 buffer solution of 300 mM KCl and 4 mM HEPES and contained a final concentration of 2uM ssODN, 5-10 uM sgRNA, and 8 uM Cas9 protein (IDT) and were injected as described above. At 3-4 dpf, injected embryos were screened by PCR for integration of the isoform-specific ssODN repair template into the respective *tjp1b* locus using a forward primer against the V5 sequence (5'-CGATTCCGAACCCGCTGCTG-3') and an isoform-specific reverse primer as follows:
tjp1b Alpha: 5'-TCCAAGAAGAGCTCAGCACG-3';
tjp1b Beta: 5'-AACCAAAAATGACACGACAGGCTTTCC-3';
tjp1b Gamma: 5'-ACCGCACATATCGACTAGCG-3'.
At 5 dpf, injected larvae were screened by immunohistochemistry for expression of V5-tjp1b isoforms.

Animals carrying V5-tagged *tjp1b/ZO1b* isoforms were developed by injecting CRISPR reagents and ssODN constructs, raising animals to adulthood, and outcrossing to wild-type animals. Progeny carrying the in-frame V5 modifications were identified by PCR and immunofluorescent staining, and stable lines were established.

Immunohistochemistry and confocal imaging
Anesthetized, 5 dpf larvae were fixed for 3 hr in 2% trichloroacetic acid in PBS (Martin et al., 2022). Fixed tissue was washed in PBS containing 0.5% Triton X-100, followed by standard blocking and antibody incubations. Primary antibody mixes included combinations of the following: rabbit anti-Cx35.5 (Fred Hutch Antibody Technology Facility, clone 12H5, 1:800), mouse IgG2A anti-Cx34.1 (Fred Hutch Antibody Technology Facility, clone 5C10A, 1:350), mouse IgG1 anti-ZO1 (Invitrogen, 33–9100, 1:350), mouse IgG2a anti-V5 (Invitrogen, R960-25, 1:500), rabbit anti-human Cx36 (Invitrogen, 36-4600, 1:500) and chicken anti-GFP (Abcam, ab13970, 1:350-1:500). All secondary antibodies were raised in goat (Invitrogen, conjugated with Alexa-405-Plus, –488, −555, or −633 fluorophores, 1:500). Tissue was then cleared stepwise in a 25%, 50%, 75% glycerol series, dissected, and mounted in ProLong Gold antifade reagent (ThermoFisher). Images were acquired on a Leica SP8 Confocal using a 405-diode laser and a white light laser set to 499, 553, 598, and 631 nm, depending on the fluorescent dye imaged. Each laser line's data was collected sequentially using custom detection filters based on the dye. Images of the Club Endings (CEs) were collected using a 63x, 1.40 numerical aperture (NA), oil immersion lens, and images of M/CoLo synapses were collected using a 40x, 1.20 NA, water immersion lens unless otherwise noted in figure legend. For each set of images, the optimal optical section thickness was used as calculated by the Leica software based on the pinhole, emission wavelengths, and NA of the lens. Within each experiment where fluorescence intensity was to be quantified, all animals were stained together using the same antibody mix, processed at the same time, and all confocal settings (laser power, scan speed, gain, offset, objective, and zoom) were identical. Multiple animals per genotype were analyzed to account for biological variation. To account for technical variation, fluorescence intensity values for each region of each animal were an average across multiple synapses.

Analysis of confocal imaging
For fluorescence intensity quantitation, confocal images were processed and analyzed using FiJi software (Schindelin et al., 2012). To quantify staining at M/CoLo synapses, a standard region of interest (ROI) surrounding each M/CoLo site of contact was drawn and the mean fluorescence intensity was measured. Standard deviations and errors were computed using Prism (GraphPad) software. Figure images were created using FiJi, Photoshop (Adobe), and Illustrator (Adobe). Unpaired t-test with Welch's correction was performed using Prism (GraphPad) to determine statistical significance. For all experiments, values were normalized to *wildtype* control animals unless otherwise noted, and n represents the number of fish used.

scRNA-seq analysis
The full methods from the embryo dissociation and cDNA library method can be found from the original dataset publication (Farnsworth et al., 2020). In short, whole larvae from the *Tg(olig2:GFP)vu12* and *Tg(elavl3:GCaMP6s)* backgrounds were pooled (n=15 per replicate), with 2 replicates at each timepoint (1, 2, 5dpf). Dissociated cells were then run on a 10X Chromium platform using 10x v.2 chemistry aiming for 10,000 cells per run. We aligned reads to the zebrafish genome, GRCz11, using the 10X Cellranger pipeline (version 3.1) using the Lukowicz-Bedford GTF (Lukowicz-Bedford et al., 2022),

which incorporates genome wide improvements (Lawson et al., 2020). Transcriptomes were analyzed using the Seurat (V3.1.5) software package for R (V4.1.0) using standard quality control, normalization, and analysis steps. Final UMAP analysis resulted in 49,367 cells with 115 PC dimensions and a resolution of 15.0, which produced 238 clusters. Complete code and data sets can be found at www.adammillerlab.com/resources.

Fluorescent RNA *in situ*

Custom RNAscope probes to target specific *tjp1b/ZO1b* isoforms were designed and ordered through ACD. For fluorescent *in situs*, we used a modified RNAscope protocol (Gross-Thebing et al., 2014). Briefly, 5 dpf embryos were fixed for 1 h at room temperature in 4% paraformaldehyde / 4% sucrose, rinsed in PBS / 0.1% Tween20, dehydrated through a methanol series and then stored in 100% methanol at −20°C at least overnight. The methanol was removed and the tissue was air dried for 30 min at room temperature. The tissue was then exposed to Protease Plus for 1 hr 15 min and washed with PBS / 0.1% Tween 20. The probe was pre-warmed at 40 °C, then cooled. Tissue was incubated with probe overnight at 40 °C. Standard RNAscope V2 multiplex reagents and Opal fluorophores were used, with the modification that 0.2X SSC / 0.1% Tween 20 was used for all wash steps. After *in situ*, tissue was rinsed in PBS / 0.1% Tween 20, then immunostained as described above with the exception that Tween 20 was used as the detergent instead of Triton X-100. Stained tissue was either mounted (whole mount) and imaged in 75% glycerol, or dissected and mounted with ProLong Gold Antifade.

qPCR analysis

RNA was isolated from 5 dpf larvae using TRIzol reagent, and 5 µg total RNA was used to synthesize cDNA using the Superscript III First strand cDNA synthesis kit (ThermoFisher). qPCR was performed using BioRad CFX Opus 96 Real-Time PCR System thermocycler with the SSsoAdvanced Universal SYBR® Green Supermix (BioRad) per manufacturer's instructions. All samples were performed in technical triplicate over three independent experiments. Relative expression of each ZO1b isoform was determined after normalizing to a reference gene using the $2^{-\Delta\Delta C_T}$ (Livak) method. Two-tailed unpaired t-test was performed using Prism (GraphPad) to determine statistical significance.

Primers were designed to bind around intron/exon boundaries and to amplify *tjp1b* isoforms. Sequences are as follows:
tjp1b Alpha, 5'-TGCTGGAGGAGGTGTGT-3' and 5'-CTGTGCGCTGGTTTAGTTTG-3' (exon 1 *Alpha* - exon 2);
tjp1b Beta, 5'-CTGTTATGCAGCTGGCTCTA-3' and 5'-AACTGCAGGGCCGTATTT-3' (exon 1 *Beta* - exon 3);
tjp1b Gamma, 5'-CCCGGGCTGCCTCTAATA-3' and 5'-CCTGTGTAGAGTTACAGTGTGC-3' (exon 1 *Gamma* - exon 5);
reference gene *eef1a1l1* (ENSDART00000167847.2), 5'-ATGGCACGGTGACAACAT-3' and 5'-CTCCAGAAGCGTAACACCATT-3' (exon 3 – exon 4).

Cell culture, transfection, and immunoprecipitation
HEK293T/17 verified cells were purchased from ATCC (CRL-11268; STR profile, amelogenin: X). Cells were expanded and maintained in Dulbecco's Modified Eagle's Medium (DMEM, ATCC) plus 10 % fetal bovine serum (FBS, Gibco) at 37 °C in a humidified incubator in the presence of 5 % CO_2. Low passage aliquots were cryopreserved and stored according to manufacturer's instructions. Cells from each thawed cryovial were monitored for mycoplasma contamination using the Universal Mycoplasma Detection Kit (ATCC, 30–1012K).

tjp1b-beta and *-gamma* full-length sequences were cloned from a cDNA library developed from 3 dpf animals using Trizol and SuperScript III, as described above for qPCR. *tjp1b-alpha* specific exons 1 and 2 were cloned from genomic DNA, and full-length cDNA was assembled using Gibson cloning techniques. *tjp1b/ZO1b-alpha* and *tjp1b/ZO1b-beta* were cloned into the pCMV expression vector with an NH_2-terminal mVenus tag and a COOH-terminal 8xHIS tag. *tjp1b/ZO1b-gamma* was cloned into the pCMV expression vector with a COOH-terminal 8xHIS tag. Cx34.1 was expressed from a pCMV vector generated in a previous study (Lasseigne et al., 2021). Low passage HEK293T/17 cells were seeded 24 hr prior to transfection (1×10^6 cells/well of a six-well dish), and the indicated plasmids were co-transfected using Lipofectamine 3000 (Invitrogen) following the manufacturer's instructions. Cells were collected 36–48 hr post-transfection and lysed in 0.25 ml solubilization buffer (50 mM Tris [pH7.4], 100 mM NaCl, 5 mM EDTA, 1.5 mM MgCl2, 1 mM DTT and 1% Triton X-100) plus a protease inhibitor cocktail (Pierce). Lysates were centrifuged at 20,000 x g for 30 min at 4°C, and equal amounts of extract were immunoprecipitated with 1.0 µg mouse anti-ZO1 (Invitrogen, 33–9100) overnight with rocking at 4°C. Immunocomplexes were captured with 25 µl prewashed Protein A/G agarose beads for 1 hr with rocking at 4°C. Beads were washed three times with lysis buffer, and bound proteins were boiled for 3 min in the presence of LDS-PAGE loading dye containing 200 mM DTT. Samples were resolved by SDS-PAGE using a 4–15% gradient gel and analyzed by Western blot using the following primary antibodies: mouse anti-ZO1 (Invitrogen, 33–9100) and rabbit anti-Cx34.1 3A4 (Fred Hutch Antibody Technology Facility, clone 3A4). Compatible near-infrared secondary antibodies were used for visualization with the Odyssey system (LI-COR).

Acknowledgments
We would like to thank and acknowledge the University of Oregon zebrafish facility staff for superb fish care, especially through the challenges of the global pandemic. We would like to thank the administrative staff at the University of Oregon Institute of Neuroscience.

Competing Interests
None to declare.

Funding
This work was supported by the NIH Eunice Kennedy Shriver National Institute of Child Health and Human Development (NICHD) Developmental Biology Training Grant

T32HD007348 to LEK and AML, the NIH National Institute of General Medical Sciences (NIGMS) Graduate Training in Genetics Grant T32GM007413 to RML, the NICHD Ruth L Kirschstein National Research Service Award F32HD102182 to EAM, the Women in Science and Math (WiSM) Academic Residential Community Summer Research Award to APK, and the National Institue of Neurological Disorders and Stroke (NINDS) Awards R21NS117967 and R01NS105758 to ACM.

References

Ackermann F, Waites CL, Garner CC. 2015. Presynaptic active zones in invertebrates and vertebrates. *EMBO Reports* **16**:923–938. doi:10.15252/embr.201540434

Alcamí P, Pereda AE. 2019. Beyond plasticity: the dynamic impact of electrical synapses on neural circuits. *Nature Reviews Neuroscience* **20**:253-271. doi: 10.1038/s41583-019-0133-5

Araki Y, Hong I, Gamache TR, Ju S, Collado-Torres L, Shin JH, Huganir RL. 2020. SynGAP isoforms differentially regulate synaptic plasticity and dendritic development. *Elife* **9**. doi:10.7554/eLife.56273

Arroyo DA, Kirkby LA, Feller MB. 2016. Retinal Waves Modulate an Intraretinal Circuit of Intrinsically Photosensitive Retinal Ganglion Cells. *Journal of Neuroscience* **36**:6892–6905. doi:10.1523/JNEUROSCI.0572-16.2016

Balda MS, Anderson JM. Two classes of tight junctions are revealed by ZO-1 isoforms. 1993. *American Journal of Physiology* **264**:C918-24. doi: 10.1152/ajpcell.1993.264.4.C918

Bartelmez GW, Hoerr NL. 1933. The vestibular club endings in ameiurus. Further evidence on the morphology of the synapse. *The Journal of Comparative Neurology* **57**:401–428.

Bhattacharya A, Aghayeva U, Berghoff EG, Hobert O. 2019. Plasticity of the Electrical Connectome of C. elegans. *Cell* **176**:1174-1189.e16. doi:10.1016/j.cell.2018.12.024

Bloomfield SA, Völgyi B. 2009. The diverse functional roles and regulation of neuronal gap junctions in the retina. *Nature Reviews Neuroscience* **10**:495–506. doi:10.1038/nrn2636

Brightman MW, Reese TS. 1969. Junctions between intimately apposed cell membranes in the vertebrate brain. *Journal of Cell Biology* **40**:648–677. doi:10.1083/jcb.40.3.648

Burger A, Lindsay H, Felker A, Hess C, Anders C, Chiavacci E, Zaugg J, Weber LM, Catena R, Jinek M, Robinson MD, Mosimann C. 2016. Maximizing mutagenesis with solubilized CRISPR-Cas9 ribonucleoprotein complexes. *Development*. doi:10.1242/dev.134809

Casafont I, Berciano MT, Lafarga M. 2010. Bortezomib Induces the Formation of Nuclear poly(A) RNA Granules Enriched in Sam68 and PABPN1 in Sensory Ganglia Neurons. *Neurotoxicity Research* **17**, 167–178. doi: 10.1007/s12640-009-9086-1

Eaton RC, Farley RD, Kimmel CB, Schabtach E. 1977. Functional development in the Mauthner cell system of embryos and larvae of the zebra fish. *Journal of Neurobiology* **8**:151–172. doi:10.1002/neu.480080207

El-Brolosy MA, Kontarakis Z, Rossi A, Kuenne C, Günther S, Fukuda N, Kikhi K, Boezio GLM, Takacs CM, Lai SL, Fukuda R, Gerri C, Giraldez AJ, Stainier DYR. 2019. Genetic compensation triggered by mutant mRNA degradation. *Nature* **568**:193-197. doi: 10.1038/s41586-019-1064-z

Farnsworth DR, Saunders LM, Miller AC. 2020. A single-cell transcriptome atlas for zebrafish development. *Developmental Biology* **459**:100–108. doi:10.1016/j.ydbio.2019.11.008

González-Mariscal L, Betanzos A, Ávila-Flores A. 2000. MAGUK proteins: structure and role in the tight junction. *Seminars in Cell & Developmental Biology* **11**:315–324. doi:10.1006/scdb.2000.0178

Goodman L, Baddeley D, Ambroziak W, Waites CL, Garner CC, Soeller C, Montgomery JM. 2017. N-terminal SAP97 isoforms differentially regulate synaptic structure and postsynaptic surface pools of AMPA receptors. *Hippocampus* **27**:668–682. doi:10.1002/hipo.22723

Grant SGN. 2019. Synapse diversity and synaptome architecture in human genetic disorders. *Human Molecular Genetics* **28**:R219–R225. doi:10.1093/hmg/ddz178

Gross-Thebing T, Paksa A, Raz E. 2014. Simultaneous high-resolution detection of multiple transcripts combined with localization of proteins in whole-mount embryos. *BMC Biology* **12**:55. doi:10.1186/s12915-014-0055-7

Hirao K, Hata Y, Yao I, Deguchi M, Kawabe H, Mizoguchi A, Takai Y. 2000. Three Isoforms of Synaptic Scaffolding Molecule and Their Characterization. *Journal of Biological Chemistry* **275**:2966–2972. doi:10.1074/jbc.275.4.2966

Jacoby J, Kimmel CB. 1982. Synaptogenesis and its relation to growth of the postsynaptic cell: a quantitative study of the developing Mauthner neuron of the axolotl. *The Journal of Comparative Neurology* **204**:364–376.

Kimmel CB, Sessions SK, Kimmel RJ. 1981. Morphogenesis and synaptogenesis of the zebrafish Mauthner neuron. *The Journal of Comparative Neurology* **198**:101-20. doi: 10.1002/cne.901980110

Kimmel CB, Ballard WW, Kimmel SR, Ullmann B, Schilling TF. 1995. Stages of embryonic development of the zebrafish. *Developmental Dynamics* **203**:253–310. doi:10.1002/aja.1002030302

Lasseigne AM, Echeverry FA, Ijaz S, Michel JC, Martin EA, Marsh AJ, Trujillo E, Marsden KC, Pereda AE, Miller AC. 2021. Electrical synaptic transmission requires a postsynaptic scaffolding protein. *Elife* **10**. doi:10.7554/eLife.66898

Lawson ND, Li R, Shin M, Grosse A, Yukselen O, Stone OA, Kucukural A, Zhu L. 2020. An improved zebrafish transcriptome annotation for sensitive and comprehensive detection of cell type-specific genes. *Elife* **9**. doi:10.7554/eLife.55792

Li X, Olson C, Lu S, Kamasawa N, Yasumura T, Rash JE, Nagy JI. 2004. Neuronal connexin36 association with zonula occludens-1 protein (ZO-1) in mouse brain and interaction with the first PDZ domain of ZO-1. *European Journal of Neuroscience* **19**:2132-46. doi: 10.1111/j.0953-816X.2004.03283.x

Liu KS, Fetcho JR. 1999. Laser Ablations Reveal Functional Relationships of Segmental Hindbrain Neurons in Zebrafish. *Neuron* **23**:325–335.

Lukowicz-Bedford RM, Farnsworth DR, Miller AC. 2022. Connexinplexity: the spatial and temporal expression of *connexin* genes during vertebrate organogenesis. *G3 Genes|Genomes|Genetics* **12**. doi:10.1093/g3journal/jkac062

Marder E. 1998. Electrical synapses: Beyond speed and synchrony to computation. *Current Biology* **8**:R795–R797. doi:10.1016/S0960-9822(07)00502-7
Marsh AJ, Michel JC, Adke AP, Heckman EL, Miller AC. 2017. Asymmetry of an Intracellular Scaffold at Vertebrate Electrical Synapses. *Current Biology* **27**:3561-3567.e4. doi:10.1016/j.cub.2017.10.011
Martin D, Tawadros T, Meylan L, Abderrahmani A, Condorelli DF, Waeber G, Haefliger JA. 2003. Critical role of the transcriptional repressor neuron-restrictive silencer factor in the specific control of connexin36 in insulin-producing cell lines. *Journal of Biological Chemistry* **278**:53082-9. doi: 10.1074/jbc.M306861200
Martin E, Ijaz S, Pereda A, Miller A. 2022. Trichloroacetic Acid Fixation and Antibody Staining of Zebrafish Larvae. *BIO-PROTOCOL* **12**. doi:10.21769/BioProtoc.4289
Martin EA, Lasseigne AM, Miller AC. 2020. Understanding the Molecular and Cell Biological Mechanisms of Electrical Synapse Formation. *Frontiers in Neuroanatomy* **14**. doi:10.3389/fnana.2020.00012
Miller AC, Pereda AE. 2017. The electrical synapse: Molecular complexities at the gap and beyond. *Developmental Neurobiology* **77**:562–574. doi:10.1002/dneu.22484
Miller AC, Whitebirch AC, Shah AN, Marsden KC, Granato M, O'Brien J, Moens CB. 2017. A genetic basis for molecular asymmetry at vertebrate electrical synapses. *Elife* **6**. doi:10.7554/eLife.25364
Moreno-Mateos MA, Vejnar CE, Beaudoin J-D, Fernandez JP, Mis EK, Khokha MK, Giraldez AJ. 2015. CRISPRscan: designing highly efficient sgRNAs for CRISPR-Cas9 targeting in vivo. *Nature Methods* **12**:982–988. doi:10.1038/nmeth.3543
Moroz LL, Kohn AB. 2016. Independent origins of neurons and synapses: insights from ctenophores. *Philosophical Transactions of the Royal Society B: Biological Sciences* **371**:20150041. doi:10.1098/rstb.2015.0041
Narcís JO, Tapia O, Tarabal O, Piedrafita L, Calderó J, Berciano MT, Lafarga M. 2018. Accumulation of poly(A) RNA in nuclear granules enriched in Sam68 in motor neurons from the SMNΔ7 mouse model of SMA. *Scientific Reports* **8**, 9646. doi.org/10.1038/s41598-018-27821-3
O'Brien J. 2019. Design principles of electrical synaptic plasticity. *Neuroscience Letters* **695**:4-11. doi: 10.1016/j.neulet.2017.09.003
Patel MR, Lehrman EK, Poon VY, Crump JG, Zhen M, Bargmann CI, Shen K. 2006. Hierarchical assembly of presynaptic components in defined C. elegans synapses. *Nature Neuroscience* **9**:1488-98. doi: 10.1038/nn1806
Pereda AE. 2014. Electrical synapses and their functional interactions with chemical synapses. *Nature Reviews Neuroscience* **15**:250–263. doi:10.1038/nrn3708
Pereda AE, Rash JE, Nagy JI, Bennett MVL. 2004. Dynamics of electrical transmission at club endings on the Mauthner cells. *Brain Research Reviews* **47**:227–244.
Ryan TJ, Grant SGN. 2009. The origin and evolution of synapses. *Nature Reviews Neuroscience* **10**:701–712. doi:10.1038/nrn2717
Satou C, Kimura Y, Kohashi T, Horikawa K, Takeda H, Oda Y, Higashijima S. 2009. Functional role of a specialized class of spinal commissural inhibitory neurons during fast escapes in zebrafish. *Journal of Neuroscience* **29**:6780–6793. doi:10.1523/JNEUROSCI.0801-09.2009
Schindelin J, Arganda-Carreras I, Frise E, Kaynig V, Longair M, Pietzsch T, Preibisch S, Rueden C, Saalfeld S, Schmid B, Tinevez J-Y, White DJ, Hartenstein V, Eliceiri K,

Tomancak P, Cardona A. 2012. Fiji: an open-source platform for biological-image analysis. *Nature Methods* **9**:676–682. doi:10.1038/nmeth.2019
Shah AN, Davey CF, Whitebirch AC, Miller AC, Moens CB. 2015. Rapid reverse genetic screening using CRISPR in zebrafish. *Nature Methods* **12**:535–540. doi:10.1038/nmeth.3360
Siddiqui TJ, Craig AM. 2011. Synaptic organizing complexes. *Current Opinion in Neurobiology* **21**:132–143. doi:10.1016/j.conb.2010.08.016
Söhl G, Maxeiner S, Willecke K. Expression and functions of neuronal gap junctions. 2005. *Nature Review Neuroscience* **6**:191-200. doi: 10.1038/nrn1627
Stevenson BR, Siliciano JD, Mooseker MS, Goodenough DA. 1986. Identification of ZO-1: a high molecular weight polypeptide associated with the tight junction (zonula occludens) in a variety of epithelia. *Journal of Cell Biology* **103**:755-66. doi: 10.1083/jcb.103.3.755
Waites CL, Specht CG, Härtel K, Leal-Ortiz S, Genoux D, Li D, Drisdel RC, Jeyifous O, Cheyne JE, Green WN, Montgomery JM, Garner CC. 2009. Synaptic SAP97 isoforms regulate AMPA receptor dynamics and access to presynaptic glutamate. *Journal of Neuroscience* **29**:4332-45. doi: 10.1523/JNEUROSCI.4431-08.2009
Willott E, Balda MS, Heintzelman M, Jameson B, Anderson JM. Localization and differential expression of two isoforms of the tight junction protein ZO-1. 1992. *American Journal of Physiology* **262**:C1119-24. doi: 10.1152/ajpcell.1992.262.5.C1119
Wilson CA, High SK, McCluskey BM, Amores A, Yan Y, Titus TA, Anderson JL, Batzel P, Carvan MJ, Schartl M, Postlethwait JH. 2014. Wild Sex in Zebrafish: Loss of the Natural Sex Determinant in Domesticated Strains. *Genetics* **198**:1291–1308. doi:10.1534/genetics.114.169284
Yao C, Vanderpool KG, Delfiner M, Eddy V, Lucaci AG, Soto-Riveros C, Yasumura T, Rash JE, Pereda AE. 2014. Electrical synaptic transmission in developing zebrafish. *Journal of Neurophysiology* **0552827**:2102–13. doi:10.1152/jn.00397.2014
Zheng C-Y, Seabold GK, Horak M, Petralia RS. 2011. MAGUKs, Synaptic Development, and Synaptic Plasticity. *The Neuroscientist* **17**:493–512. doi:10.1177/1073858410386384
Zhu J, Shang Y, Zhang M. 2016. Mechanistic basis of MAGUK-organized complexes in synaptic development and signalling. *Nature Reviews Neuroscience* **17**:209–223. doi:10.1038/nrn.2016.18

Figure Legend:

Figure 1. Alternatively initiated isoforms *tjp1b/ZO1b-Beta* and *tjp1b/ZO1b-Gamma* are expressed in the Mauthner cell circuit and localize to electrical synapses. A. Schematic diagram of the *tjp1b/ZO1b* gene locus on chromosome 25: 32,031,536-32,271,394 (GRCz11 Ensembl) showing the exon structure located on the forward strand. Horizontal black bar represents the DNA strand and vertical black bars represent individual exons. The region containing alternatively initiated exons for *tjp1b/ZO1b-Alpha*, *-Beta*, and *-Gamma* isoforms is expanded between the dashed lines (Chromosome 25: 32,031,536-32,208,713). Unique initiation exons are represented by

white boxes (Exons 1 *Alpha*, 1 *Beta*, and 1 *Gamma*), additional exons are represented by grey boxes, and the first shared exon is represented by a black box (Exon 5). Lengths of exons and introns are indicated. The isoform null mutations generated by CRISPR/Cas9 for each single and double mutant line (b# designates alleles) are indicated below each Exon 1 (white box). Symbols indicate deletion (Δ) or insertion (▽) of the indicated number of base pairs. The location of the in-frame V5 epitope tag for each isoform is indicated in magenta above each Exon 1. **B.** Schematic diagram representing the alternatively initiated *tjp1b/ZO1b* isoform mRNAs *tjp1b/ZO1b-Alpha* (ENSDART00000173656.2; 7618 bp), -*Beta* (ENSDART00000155992.3; 7626 bp) and -*Gamma* (ENSDART00000112588.5; 7408 bp). Unique 5'UTRs and initiation exons are represented by white boxes, additionally spliced exons are represented by grey boxes and exons shared by all three isoforms are represented by black boxes (Exons 5-31). Approximate location of the ATG start codon and the shared TGA stop codon are indicated in each transcript. **C.** Schematic diagram of the ZO1b isoform proteins representing ZO1b-Alpha (2005 aa), -Beta (1853 aa), and -Gamma (1689 aa). The unique N-terminal amino acid sequences are indicated in the dashed box. Note that ZO1b-Alpha and ZO1b-Beta both contain amino acid sequence derived from exons 3 and 4. Domains are depicted as white shapes; CARD, PDZ, SH3, GUK and ZU5 are protein-protein interaction modules. White bars represent regions derived from unique initiation exons, grey bars represent regions derived from additionally spliced exons and black bars represent regions derived from shared exons. **D-K.** Confocal images of fluorescent RNA *in situ* (white) for the negative control *DapB* (**D, E**), *tjp1b/ZO1b-Alpha* (**F, G**)*, tjp1b/ZO1b-Beta* (**H, I**), and *tjp1b/ZO1b-Gamma* (**J, K**) in the Mauthner circuit cell bodies of 5 days post fertilization (dpf) *zf206Et* zebrafish larvae from *wildtype* (*wt*). Animals are co-stained with anti-GFP (green). Scale bars = 2 µm. Images of the Mauthner cell body (D, F, H, J) are maximum intensity projections of ~15-30 µm. Boxed regions are enlarged in D', F', H' and J' and neighboring panels show individual channels. Images of the CoLo cell body (E, G, I, K) are maximum intensity projections of ~6-12 µm and neighboring panels show individual channels. The green dashed line in the probe channel indicates the outline of the CoLo cell body. In G, the arrow indicates the *Alpha* signal in unidentified nearby cells. In H-K, the *Beta* and *Gamma* signals appear as discrete nuclear granules in the neuronal cell body (Casafont et al., 2010; Narcís et al., 2018). **L-O.** Confocal images of Mauthner circuit neurons and stereotypical electrical synaptic contacts in 5dpf *zf206Et* zebrafish larvae from heterozygous *V5-tjp1b/ZO1b Beta* (**L, M**) and heterozygous *V5-tjp1b/ZO1b-Gamma* (**N, O**) animals. Animals are stained with anti-GFP (green), anti-Cx35.5 (cyan), anti-Cx34.1 (yellow), and anti-V5 (magenta). Scale bars = 2 µm. Images of the lateral dendrite in the hindbrain (L, N) are maximum intensity projections of ~5-6 µm. Neighboring panels show individual channels. Images of the sites of contact of M/CoLo processes in the spinal cord (M, O) are maximum-intensity projections of ~3-4 µm collected using a 63x, 1.40 numerical aperture (NA), oil immersion lens. Boxed regions denote stereotyped location of electrical synapses and regions are enlarged in neighboring panels. In M' and O', the white dashed circle denotes the location of the M/CoLo site of contact. Neighboring panels show individual channels. Anterior is up in all images.

Figure 2. ZO1b-Beta is necessary for robust Connexin localization to electrical synapses. A-J. Confocal images of Mauthner circuit neurons and stereotypical electrical synaptic contacts in 5 days post fertilization (dpf) *zf206Et* zebrafish larvae from *wt* (**A, B**), *tjp1b/ZO1b-pan*$^{-/-}$ (**C, D**), *tjp1b/ZO1b-alpha*$^{-/-}$ (**E, F**), *tjp1b/ZO1b-beta*$^{-/-}$ (**G, H**), and *tjp1b/ZO1b-gamma*$^{-/-}$ (**I, J**) animals. Animals are stained with anti-GFP (green), anti-Cx35.5 (cyan), anti-Cx34.1 (yellow), and anti-ZO1 (magenta). Scale bars = 2 µm. Boxed regions denote stereotyped location of electrical synapses and regions are enlarged in neighboring panels. Images of the Mauthner cell body and lateral dendrite in the hindbrain (A, C, E, G, I) are maximum intensity projections of ~10-20 µm. In A', C', E', G', and I', images are maximum-intensity projections of ~3-6 µm and neighboring panels show the individual channels. Images of the sites of contact of M/CoLo processes in the spinal cord (B, D, F, H, J) are maximum-intensity projections of ~6-8 µm. In B', D', F', H' and J', images are from a single 0.42 µm Z-plane and the white dashed circle denotes the location of the M/CoLo site of contact. Neighboring panels show individual channels. Anterior up. **K.** Quantification of Cx34.1 fluorescence intensities at M/CoLo synapses for the noted genotypes. The height of the bar represents the mean of the sampled data normalized to the *wt* average. Circles represent the normalized value of each individual animal. *wt* n=11; *tjp1b/ZO1b-pan*$^{-/-}$ n=3, p<0.0001, ****; *tjp1b/ZO1b-alpha*$^{-/-}$ n=5, p=0.1005, ns; *tjp1b/ZO1b-beta*$^{-/-}$ n=5, p<0.0001, ****; *tjp1b/ZO1b-gamma*$^{-/-}$ n=5, p=0.7453, ns. Error bars are ± SEM. In K inset box, the height of the bar represents the mean of the sampled data normalized to the *tjp1b/ZO1b-beta*$^{-/-}$ average. Circles represent the normalized value of each individual animal. *tjp1b/ZO1b-beta*$^{-/-}$ n=6; *tjp1b/ZO1b-beta-gamma*$^{-/-}$ n=6 p=0.0023, **. Error bars are ± SEM.

Figure 3. ZO1b-Beta is sufficient for robust Connexin localization to electrical synapses. A-H. Confocal images of Mauthner circuit neurons and stereotypical electrical synaptic contacts in 5 days post fertilization (dpf) *zf206Et* zebrafish larvae from *wt* (**A, B**), *tjp1b/ZO1b-alpha-gamma*$^{-/-}$ double mutant (**C, D**), *tjp1b/ZO1b-alpha-beta*$^{-/-}$ double mutant (**E, F**), and *tjp1b/ZO1b-alpha-gamma*$^{-/-}$ double mutant (**G, H**) animals. Animals are stained with anti-GFP (green), anti-Cx35.5 (cyan), anti-Cx34.1 (yellow), and anti-ZO1 (magenta). Scale bars = 2 µm. Boxed regions denote stereotyped location of electrical synapses and regions are enlarged in neighboring panels. Images of the Mauthner cell body and lateral dendrite in the hindbrain (A, C, E and G) are maximum intensity projections of ~10-25 µm. In A', C', E' and G', images are maximum-intensity projections of ~3-7 µm and neighboring panels show the individual channels. Images of the sites of contact of M/CoLo processes in the spinal cord (B, D, F and H) are maximum-intensity projections of ~3-7 µm. In B', D', F' and H', images are from a single 0.42 µm Z-plane and the white dashed circle denotes the location of the M/CoLo site of contact. Neighboring panels show individual channels. Anterior up. **I.** Quantification of Cx34.1 fluorescence intensities at M/CoLo synapses for the noted genotypes. The height of the bar represents the mean of the sampled data normalized to the *wt* average. Circles represent the normalized value of each individual animal. *wt* n=15; *tjp1b/ZO1b-alpha-gamma*$^{-/-}$ n=5, p=0.0186, *; *tjp1b/ZO1b-alpha-beta*$^{-/-}$ n=5, p<0.0001, ****; *tjp1b/ZO1b-beta-gamma*$^{-/-}$ n=5, p<0.0001, ****. Error bars are ± SEM.

Figure S1. Characterization of ZO1b isoform tissue expression. A. scRNA-seq dataset of *tjp1b/ZO1b* expression in early development where grey represents low expression and magenta represents the highest level of expression. Cell are derived from whole embryos at 1, 2, and 5 days post fertilization (dpf) and graphed together in UMAP space. Annotated cell types of clusters are indicated and each dot represents a single cell. **B.** Confocal tile scan of fluorescent RNA *in situ* in whole 5 dpf *wt* zebrafish larvae for negative control *DapB*, *tjp1b/ZO1b-Alpha, tjp1b/ZO1b-Beta*, and *tjp1b/ZO1b-Gamma*. Images are maximum intensity projections of ~68-98 µm. Anterior left. Contrast is inverted for clarity. Black arrowhead denotes signal in spinal cord. Black arrow denotes signal in hindbrain. While there is possible expression of all three isoforms in the vacuolar cells of the notochord as notochord expression was detected by scRNA-seq methods (Fig. S1A), we note that the fluorescent RNA *in situ* method often non-specifically detects signal in the notochord (blue arrowheads). Scale bar = 20 µm. **C.** Detection of V5-N-terminal tag integration by CRISPR/Cas9 mediated HDR using a short, single-stranded nucleotide repair oligo. Genomic DNA prepared from individual injected 5 dpf zebrafish was analyzed for successful integration by PCR using a forward primer against the V5 tag and a reverse primer outside the modified region. Products for V5-Alpha (top), V5-Beta (middle) and V5-Gamma (bottom) were resolved by agarose gel electrophoresis (indicated by black arrows). Non-specific products are indicated with an asterisk (*). U = uninjected siblings, NTC = no template control. The table shows the percentage of siblings positive for integration and the percentage of siblings positive for V5 immunostain at any body location in the animal, indicating mosaic expression of V5-tagged ZO1b isoforms. **D,E.** Confocal images of the sites of contact of Mauthner/CoLo processes in the spinal cord of 5 dpf zebrafish larvae mosaically expressing V5-tjp1b/ZO1b-Beta (D) and V5-tjp1b/ZO1b-Gamma (E). V5-tjp1b/ZO1b-Beta animals are stained with anti-Cx35.5 (white), and anti-V5 (magenta). V5-tjp1b/ZO1b-Gamma animals are stained with anti-Cx36 (white), and anti-V5 (magenta). Anterior up. Scale bars = 2 µm. Images are maximum-intensity projections of ~3-4 µm and the dashed circle denotes the M/CoLo site of contact. Neighboring panels show individual channels. **F,G.** Confocal images of spinal cord floor plate collected from heterozygous V5-tjp1b/ZO1b-Beta (**F**) and heterozygous V5-tjp1b/ZO1b-Gamma (**G**) animals. Animals are stained with anti-V5 (magenta). Scale bars = 2 µm. Images are maximum-intensity projections of ~4 µm. Anterior left. **H.** Confocal tile scan of zebrafish brain from 5 dpf *zf206Et* zebrafish larvae from *V5-tjp1b/ZO1b-Beta* animals. Images are maximum intensity projections of ~42 µm. Animals are stained with anti-GFP (green), anti-V5 (magenta), and anti-Cx36 (white). Scale bars = 20 µm. Boxed region denotes stereotyped location of electrical synapses where V5-ZO1b-Beta and Cx36 overlap, and the region is enlarged in neighboring panels. White arrows denote regions where V5-ZO1b-Beta and Cx36 do not overlap. Anterior left. In H', neighboring panels show individual channels.

Figure S2. Characterization of unique regions of ZO1b isoforms. A. Amino acid sequence alignment of unique N-termini from ZO1b isoforms. Amino acids in grey are unique to each isoform, and amino acids in black are shared between isoforms. Amino acids in black underline indicate the beginning of the sequence common to all isoforms (encoded by exons 5-31; full sequence not shown). The grey box outlining amino acids

in ZO1b-Alpha indicates the CARD domain. **B.** ZO1b isoform interaction with Cx34.1. HEK293T/17 cells were transfected with plasmids to express Cx34.1 and empty vector (lane 1), ZO1b-Alpha (lane 2), ZO1b-Beta (lane 3), or ZO1b-Gamma (lane 4). Lysates were immunoprecipitated with anti-ZO1 antibody and analyzed by immunoblot for the presence of ZO1b isoform (upper) using anti-ZO1 antibody and Cx34.1 protein using Cx34.1-specific antibody (middle). Total extracts (bottom, 5% input) were blotted for Cx34.1 to demonstrate equivalent expression. Results are representative of three independent experiments. **C.** qPCR analysis of ZO1b isoform mRNA levels in *wt* and *tjp1b/ZO1b-beta*$^{-/-}$ mutants. Relative expression of each ZO1b isoform was determined after normalizing to a reference gene using the $2^{-\Delta\Delta C_T}$ (Livak) method. The height of the bar represents the relative fold-expression in *tjp1b/ZO1b-beta*$^{-/-}$ mutants compared to *wt* for each *tjp1b/ZO1b* isoform, as labeled. Circles represent results of three independent experiments. Transcriptional upregulation of each isoform is observed. Note that the *tjp1b/ZO1b-Beta* CRISPR transcript does not undergo nonsense mediated decay. *wt* n=3 (represented as the dotted line to indicate the normalized fold-value of 1 for every group); *tjp1b/ZO1b-Alpha* n=3, p=0.0472, *; *tjp1b/ZO1b-Beta* n=3, p=0.234, *; *tjp1b/ZO1b-Gamma* n=3, p=0.232, *. Two-tailed unpaired t-test was used to calculate the p value. Error bars are ± SEM.

Fig. 1

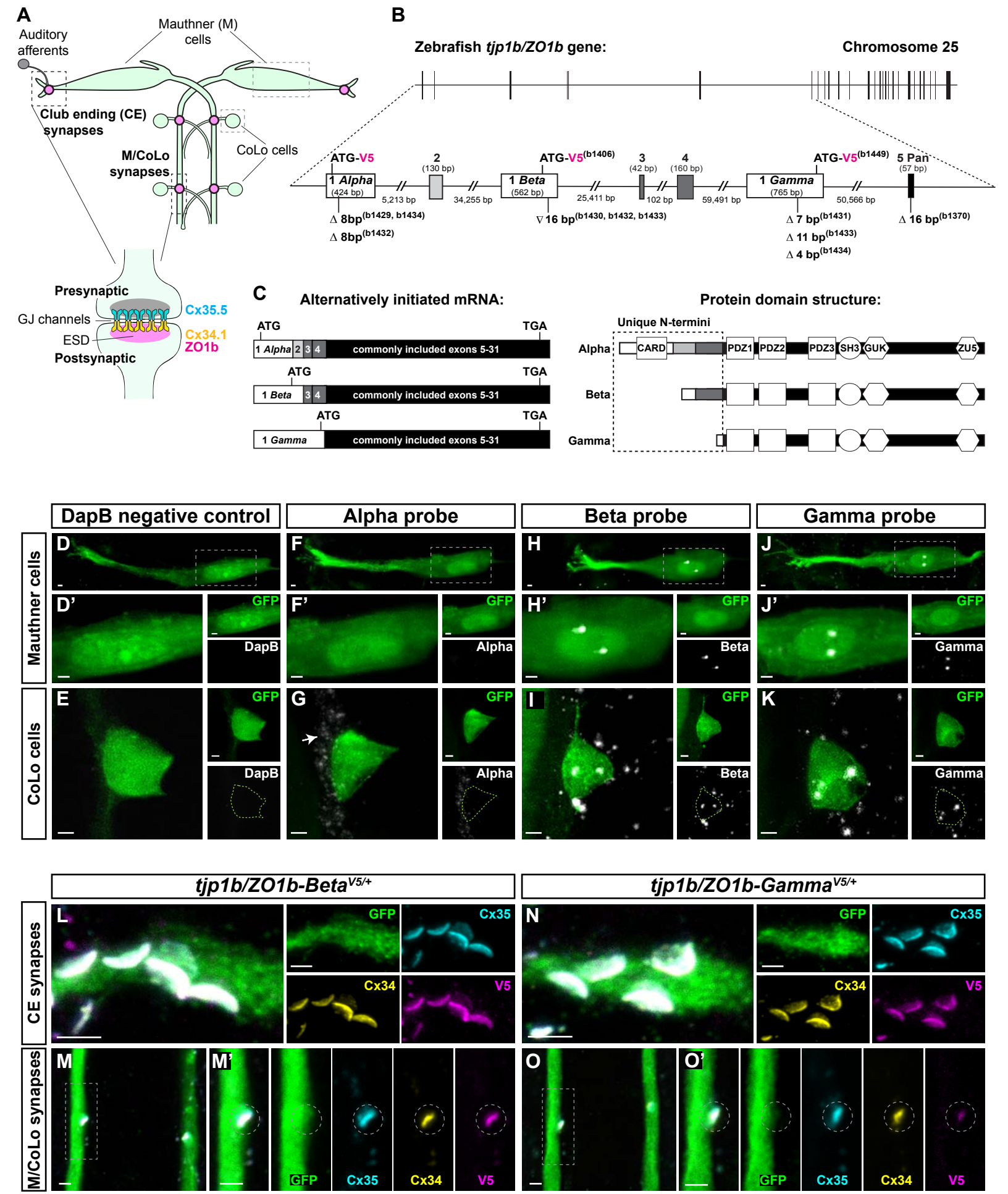
A
Auditory afferents
Mauthner (M) cells
Club ending (CE) synapses
M/CoLo synapses
CoLo cells
Presynaptic
GJ channels
ESD
Postsynaptic
Cx35.5
Cx34.1
ZO1b
B
Zebrafish tjp1b/ZO1b gene:
Chromosome 25
ATG-V5
1 Alpha (424 bp)
2 (130 bp)
ATG-V5(b1406)
1 Beta (562 bp)
3 (42 bp)
4 (160 bp)
ATG-V5(b1449)
1 Gamma (765 bp)
5 Pan (57 bp)
5,213 bp
34,255 bp
25,411 bp
102 bp
59,491 bp
50,566 bp
Δ 8bp(b1429, b1434)
Δ 8bp(b1432)
∇ 16 bp(b1430, b1432, b1433)
Δ 7 bp(b1431)
Δ 11 bp(b1433)
Δ 4 bp(b1434)
Δ 16 bp(b1370)
C
Alternatively initiated mRNA:
ATG
TGA
1 Alpha 2 3 4
commonly included exons 5-31
1 Beta 3 4
1 Gamma
Protein domain structure:
Unique N-termini
Alpha
Beta
Gamma
CARD
PDZ1
PDZ2
PDZ3
SH3
GUK
ZU5
DapB negative control
Alpha probe
Beta probe
Gamma probe
Mauthner cells
CoLo cells
D
D'
E
F
F'
G
H
H'
I
J
J'
K
GFP
DapB
Alpha
Beta
Gamma
tjp1b/ZO1b-Beta V5/+
tjp1b/ZO1b-Gamma V5/+
CE synapses
M/CoLo synapses
L
M
M'
N
O
O'
Cx35
Cx34
V5

Fig. 2

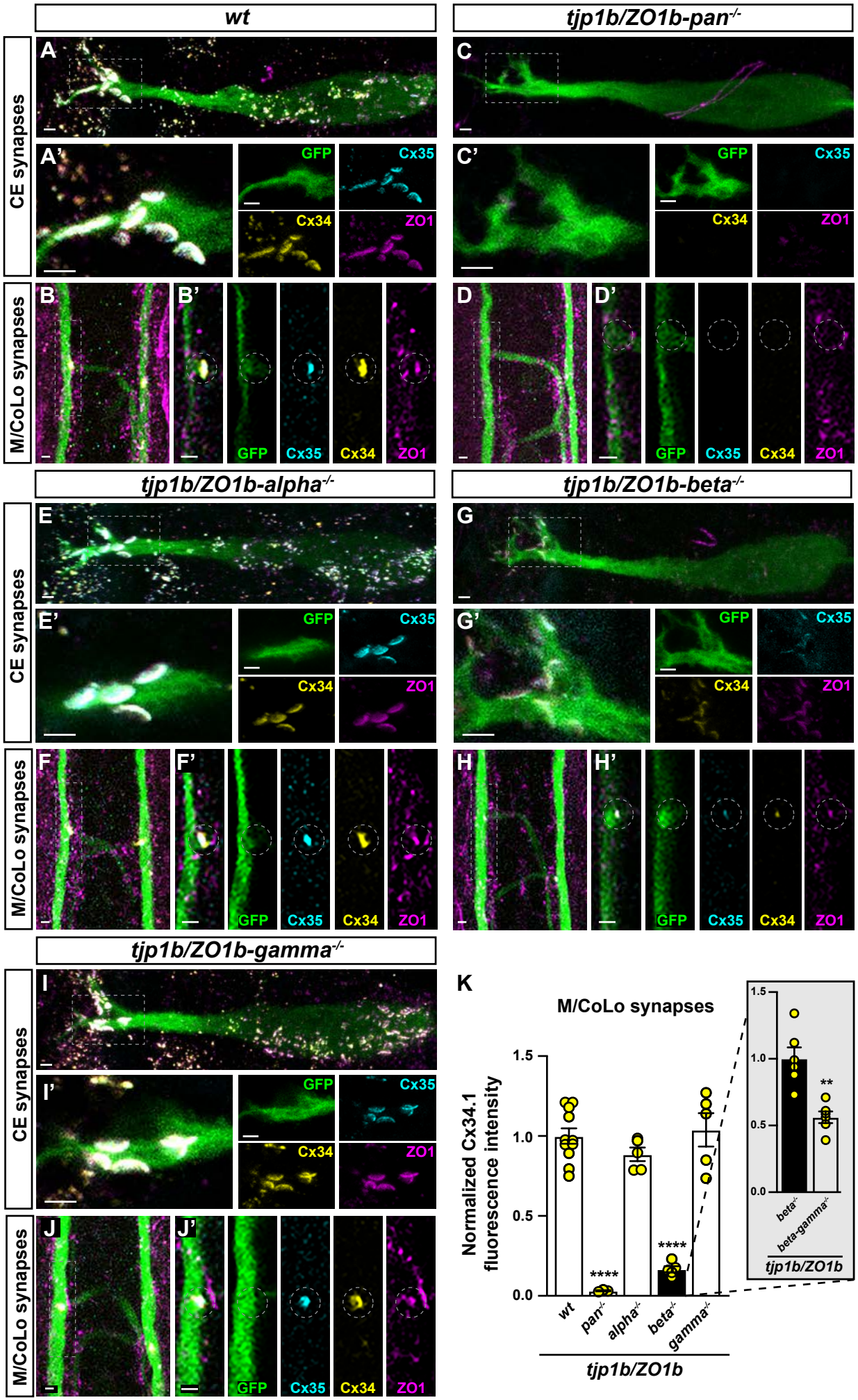
wt
tjp1b/ZO1b-pan-/-
tjp1b/ZO1b-alpha-/-
tjp1b/ZO1b-beta-/-
tjp1b/ZO1b-gamma-/-
CE synapses
M/CoLo synapses
A
A'
B
B'
C
C'
D
D'
E
E'
F
F'
G
G'
H
H'
I
I'
J
J'
GFP
Cx35
Cx34
ZO1
K
M/CoLo synapses
Normalized Cx34.1 fluorescence intensity
1.5
1.0
0.5
0.0
****
**
wt
pan-/-
alpha-/-
beta-/-
gamma-/-
tjp1b/ZO1b
beta-/-
beta-gamma-/-

Fig. 3

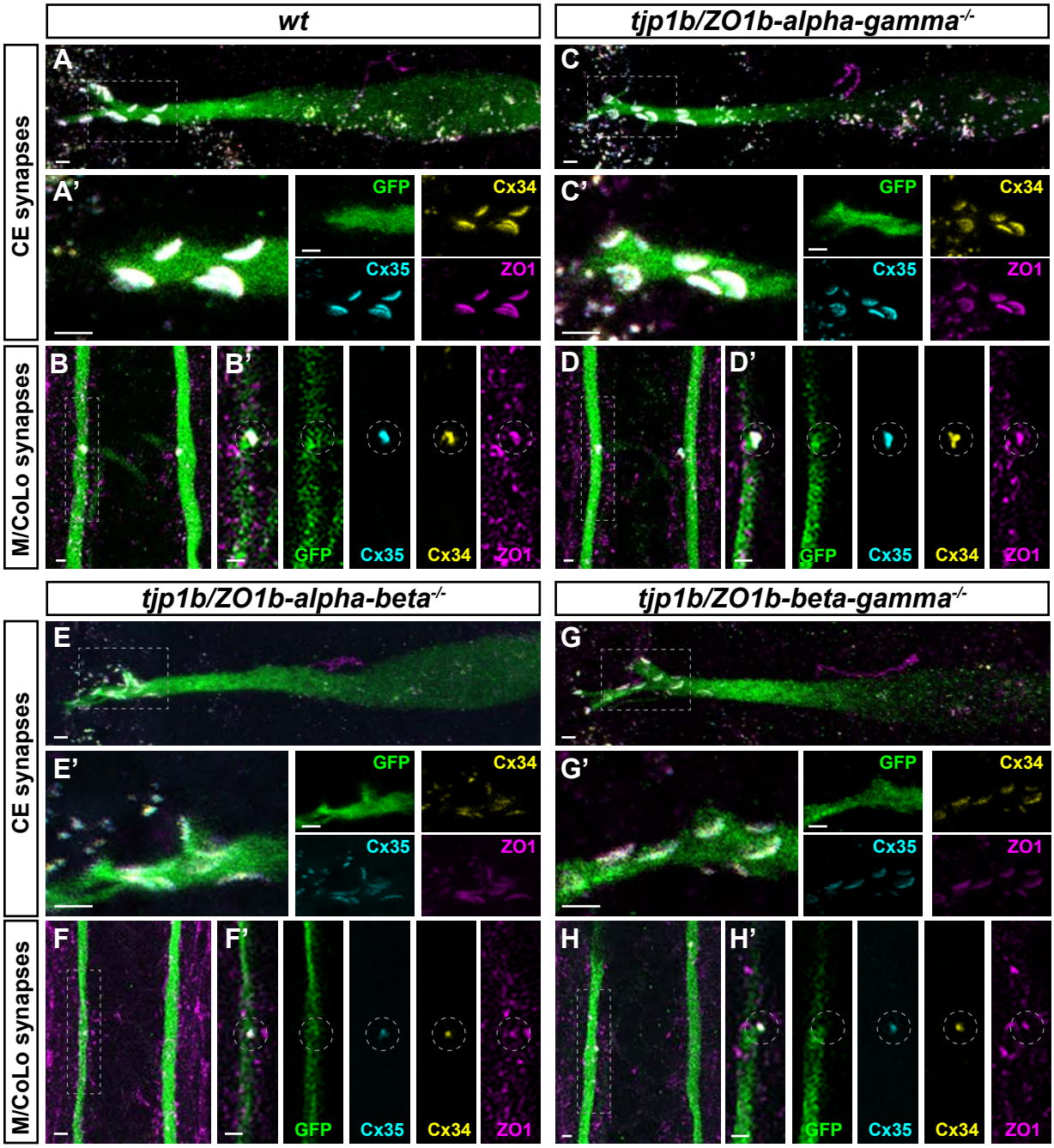
wt
tjp1b/ZO1b-alpha-gamma-/-
tjp1b/ZO1b-alpha-beta-/-
tjp1b/ZO1b-beta-gamma-/-
CE synapses
M/CoLo synapses
A
A'
B
B'
C
C'
D
D'
E
E'
F
F'
G
G'
H
H'
GFP
Cx34
Cx35
ZO1

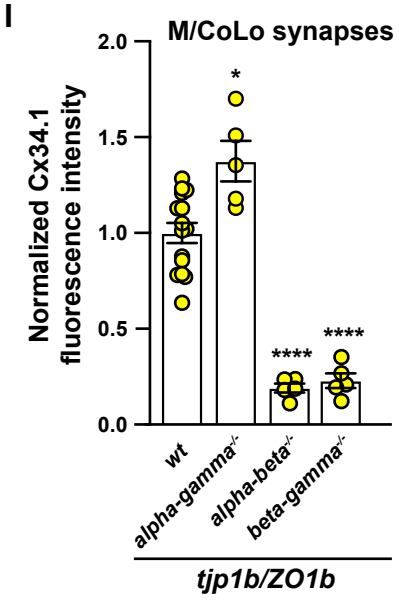
I
M/CoLo synapses
Normalized Cx34.1 fluorescence intensity
2.0
1.5
1.0
0.5
0.0
*
****
****
wt
alpha-gamma-/-
alpha-beta-/-
beta-gamma-/-
tjp1b/ZO1b

Fig. S1

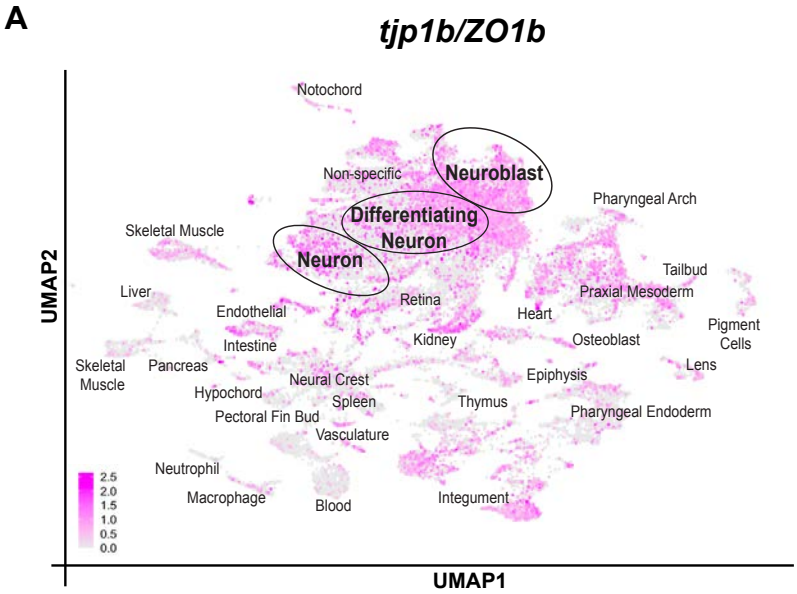

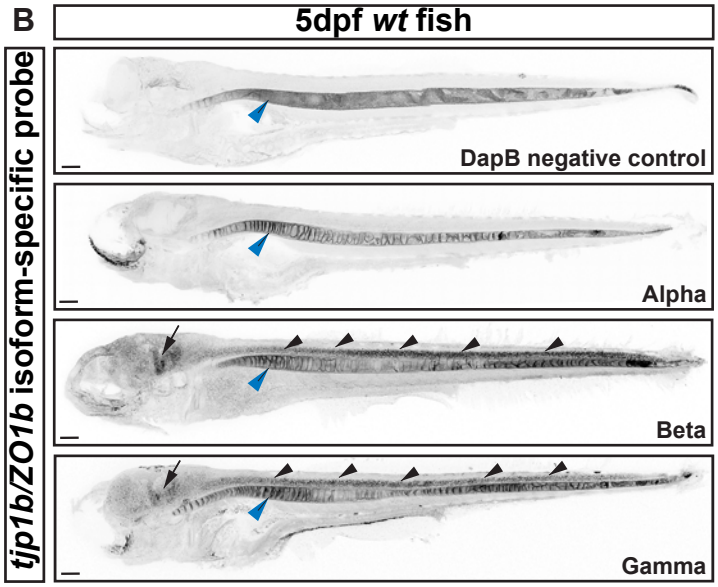

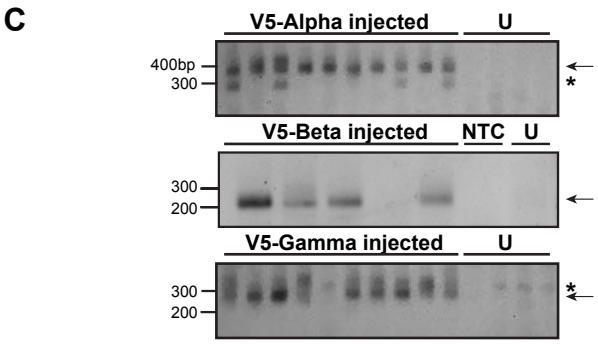

Mosaic injection	Positive PCR	α-V5 staining
V5-Alpha	10/10 (100%)	0/113 (0%)
V5-Beta	4/5 (80%)	4/18 (22%)
V5-Gamma	9/10 (90%)	65/116 (56%)

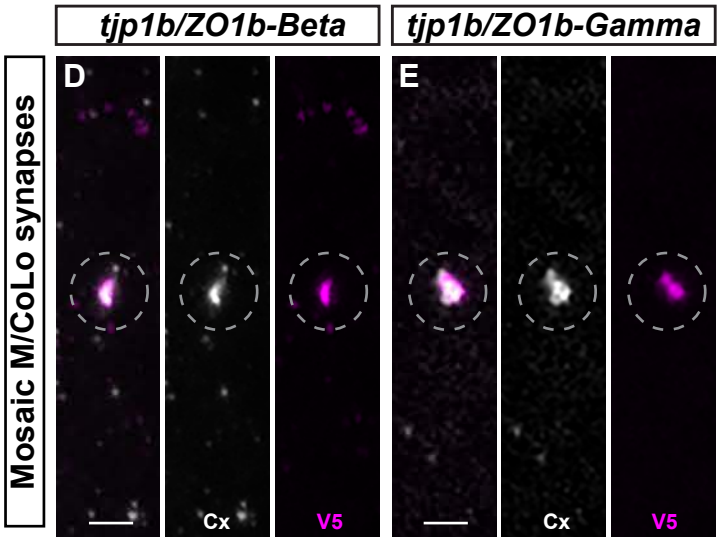

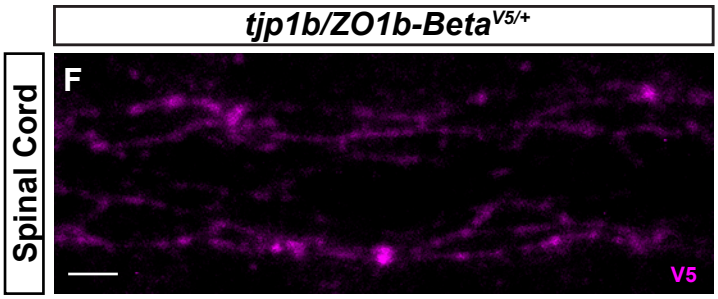

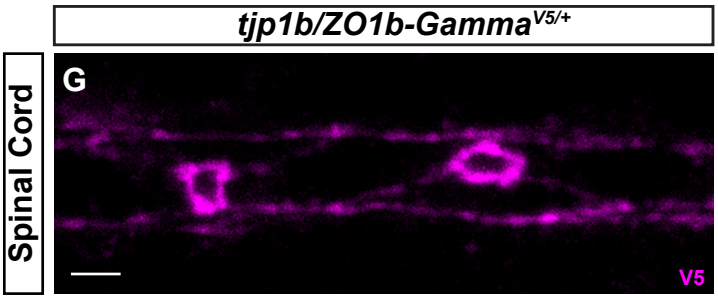

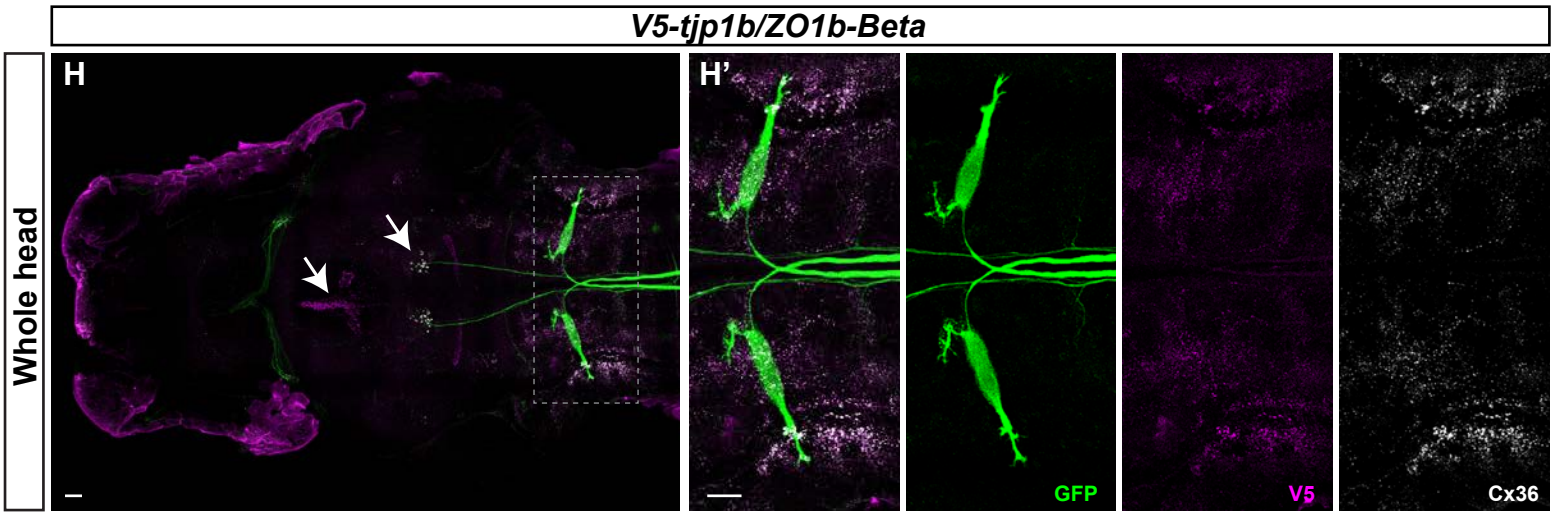

Fig. S2

A

```
ZO1b Alpha  MLLSVFGGPVEEVLAGLLKLKMFGSGSKKWFIKKNKRQRTKVQRKPASGRR  51
ZO1b Beta   --------------------------------------------------  -
ZO1b Gamma  --------------------------------------------------  -

ZO1b Alpha  NKRVSRVLKRHKEVIVKQLDVSKVLPTLVYERVFTLGEYKEILGQDSSGKR  102
ZO1b Beta   --------------------------------------------------  -
ZO1b Gamma  --------------------------------------------------  -

ZO1b Alpha  AELFLDLLSQKEPAAFSAFCGVLEEVCPHLLTCFLLDGTDGSAGENKKQGQ  153
ZO1b Beta   --------------------------------------------------  -
ZO1b Gamma  --------------------------------------------------  -

ZO1b Alpha  -TKPAHSQQNALSKGQDTVCFPPMYTDPLFDTRVFPKHDKDKYGPAVYYPK  203
ZO1b Beta   MVNYQKYITVMQLALGVTAYNRDRSLPPRKHMWVFPKHDKDKYGPAVYYPK  51
ZO1b Gamma  --------------------------------------------------  -

ZO1b Alpha  FNAYIPNPDKVSVLDESEGSGHGKPSLRRIKGRIHRSKSLDSIDLLDSNSA  254
ZO1b Beta   FNAYIPNPDKVSVLDESEGSGHGKPSLRRIKGRIHRSKSLDSIDLLDSNSA  102
ZO1b Gamma  ----------------------------------------MSARAASNKSA   11
```

B

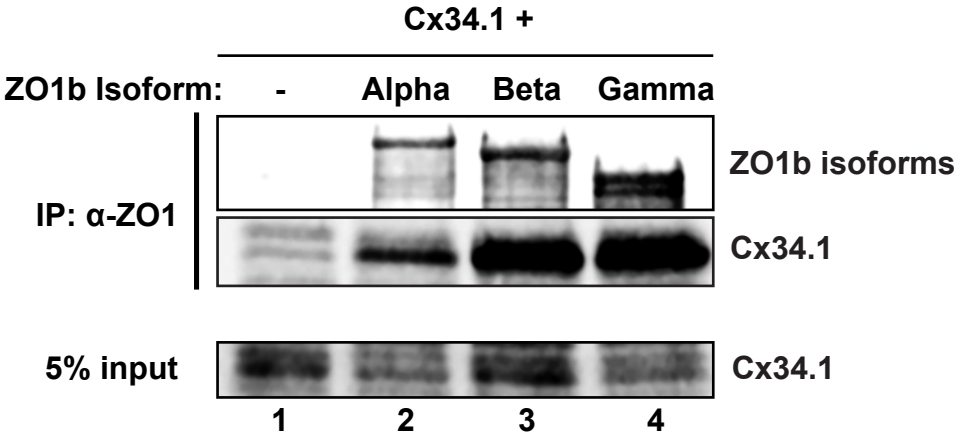
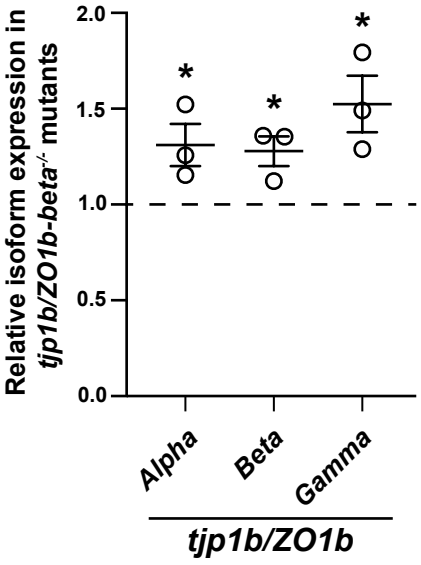
C